From intermolecular interaction energies and observable shifts to component contributions and back again: A tale of variational energy decomposition analysis.

Yuezhi Mao,[1] Matthias Loipersberger,[1] Paul R. Horn,[1] Akshaya Das,[1,2], Omar Demerdash,[1,2] Daniel S. Levine,[1] Srimukh Prasad Veccham,[1] Teresa Head-Gordon,[1,2], Martin Head-Gordon[1,3]

[1]Pitzer Theory Center and Department of Chemistry, University of California, Berkeley, CA 94720, USA
[2]Department of Bioengineering and Chemical and Biomolecular Engineering, University of California, Berkeley, CA 94720 USA
[3]email: mhg@cchem.berkeley.edu

Ann. Rev. Phys. Chem. YYYY. AA:1–28

https://doi.org/10.1146/((please add article doi))

Keywords

Density Functional Theory, Energy Decomposition Analysis, Intermolecular Interactions, Hydrogen Bonding, Dative Bonds, Radical-Molecule Complex, Force fields

Abstract

Quantum chemistry in the form of density functional theory (DFT) calculations is a powerful numerical experiment for predicting intermolecular interaction energies. However no chemical insight is gained in this way beyond predictions of observables. Energy decomposition analysis (EDA) can quantitatively bridge this gap by providing values for the chemical drivers of the interactions, such as permanent electrostatics, Pauli repulsion, dispersion, and charge transfer. These energetic contributions are identified by performing DFT calculations with constraints that disable components of the interaction. The second generation version of the absolutely localized molecular orbital EDA (ALMO-EDA-II) is described. The effect of different physical contributions on changes in observables such as structure, vibrational frequencies etc, upon complex formation is achieved via the adiabatic EDA. Several example applications are described: red versus blue-shifting hydrogen bonds, the bonding and frequency shifts of CO, N_2, and BF bound to a $[Ru(II)(NH_3)_5]^{2+}$ moiety, and the nature of the strongly bound complexes between pyridine and the benzene and naphthalene radical cations. Additionally, the use of ALMO-EDA-II to benchmark and assist in the development of advanced force fields for molecular simulation is illustrated with the recent, very promising, MB-UCB potential.

Contents

1. INTRODUCTION

There is no denying the success of modern electronic structure theory as a tool for calculating intermolecular interactions: accurate wavefunction methods such as coupled cluster theory (e.g. CCSD(T)) at the complete basis set (CBS) limit show errors that are typically much less than 1 kJ/mol. Today, the best density functionals also have very good numerical performance, with error bars that are typically on the order of 1 kJ/mol (1, 2). While early functionals failed to account for long-range dispersion interactions, this problem has been solved by the development of damped C6 potential functions (e.g. the -D2 and D3 corrections (3)), and Van der Waals density functionals such as VV10 (4).

Such methods are reliable numerical experiments that tell us the strength, ΔE_{INT}, of an intermolecular interaction between fragments (F) such as a hydrogen bond between two water molecules:

$$\Delta E_{\mathrm{INT}} = E_{\mathrm{FULL}} - \sum_{F} E_F \qquad 1.$$

However, this still leaves the basic question: "What *is* a hydrogen or halogen bond, actually?" Today, one can find advocates for an electrostatic picture(5, 6) of the hydrogen bond (dipole-dipole interactions, or driven by the electrostatic potential), all the way to advocates of a "resonance" picture(7, 8) where hydrogen bonds are entirely driven by donor-acceptor interactions. In this article, we take up the development of a framework for energy decomposition analysis (EDA) of DFT calculations that addresses questions of the physical origin of intermolecular interactions in a mathematically well-defined way.

Any interpretation of intermolecular interactions must contain terms corresponding to the different contributions that are known to arise in the long-range *non-overlapping* limit.(9) These include (i) permanent electrostatics (charge-charge, charge-dipole, dipole-dipole, etc), which may be either attractive or repulsive, (ii) attractive induced electrostatics or polarization (beginning with induced dipoles), and (iii) the attractive dispersion interaction, representing long-range correlated electron fluctuations. Which of these terms is dominant at long distance can often be discerned from the distance dependence of the calculated interaction energy.

However, interesting non-bonded interactions are usually in the *overlapping* regime, where two other chemically familiar effects come into play. These are, (iv) Pauli repulsion between filled orbitals that begin to overlap, and (v) donor-acceptor interactions between filled orbitals on one species and empty orbitals on the other. These two contributions both depend on the overlap between interacting species, which decays exponentially. This scaling difference provides a basic reason why these contributions are potentially separable from the polynomially decaying long-range terms (i)-(iii). A schematic representation of these different physical contributions to intermolecular interactions is shown in **Figure 1**.

EDA aims to deconstruct or separate a net interaction energy into physically meaningful constituent parts such as **Figure 1**. This will typically be done by defining a sequence of constrained intermediate states which selectively disable fewer and fewer physical components of the interaction, such as polarization and/or charge-transfer. In the case of the EDA discussed in this work(10), we will distinguish 5 separate states of the electrons: separate fragments (E_F for each fragment F) at their optimal geometry and their geometry in the complex, a "frozen complex" (E_{FRZ}), a "polarized complex" (E_{POL}), and the fully relaxed complex (E_{FULL}). Thus Eq. 1 can be recast as the difference between each consecutive pair of these 5 states:

$$\Delta E_{\mathrm{INT}} = \Delta E_{\mathrm{GD}} + \Delta E_{\mathrm{FRZ}} + \Delta E_{\mathrm{POL}} + \Delta E_{\mathrm{CT}} \qquad 2.$$

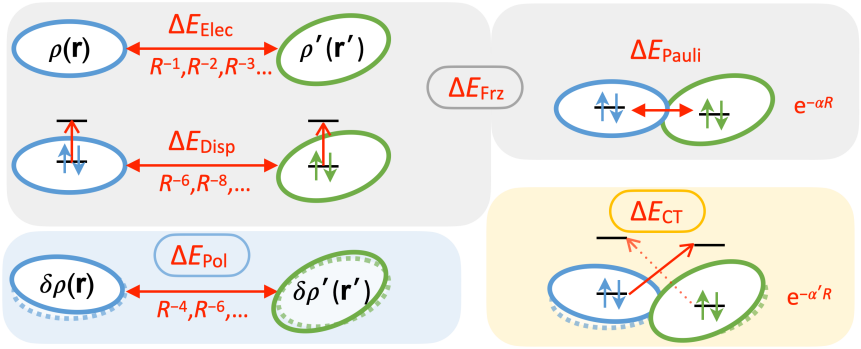

Figure 1

A schematic diagram of the five main physical contributions to intermolecular interactions. Shown on the left are three contributions that are present at long-range (permanent electrostatics, dispersion and polarization). Shown on the right are the two other contributions (Pauli repulsion and charge-transfer) that are significant when the electron densities of interacting molecules overlap with each other. EDA aims to make useful definitions of these contributions at all separations, such that all change smoothly to their correct long-range limits. The shading indicates how the contributions are grouped into ΔE_{FRZ}, ΔE_{POL}, and ΔE_{CT} in Eq. 2.

The initial reference, rather than being isolated electrons and nuclei, will be non-interacting *molecules*. Subsequent intermediate states are *partially* interacting, with constraints such as frozen electronic degrees of freedom (orbitals) to separate the different physical components of the interaction in the overlapping regime. Such states, even though not experimentally observable, should obey all quantum mechanical postulates, to ensure the energy differences between them are physically meaningful.

At the outset we must recognize a non-uniqueness problem. For a chosen electronic structure model, the final calculated interaction energy is independent of the *path* through intermediate states taken by any analysis. However, the constrained intermediate states are not uniquely defined, and therefore multiple definitions are possible. This makes EDA controversial, because one may feel that the resulting contributions delineated for instance in Eq. 2 are not useful because of non-uniqueness (11). If so, should one ignore all efforts at EDA? In fact, there are good reasons not to make such a judgement. First, experimental observables are often signatures of particular physical interactions captured in Eq. 2. For example, the common red shift in the OH frequency of the hydrogen bond or CO ligated to a metal is intuitively identified with CT. Thus, as we will illustrate, a useful EDA can help identify the physical origin of *observable effects*. An important implication that we shall also discuss later is that EDA terms contribute to reliably representing those physical concepts in molecular mechanics force fields.

There are also sensible criteria that can be used to guide the design of a useful EDA (and to distinguish good ones from those with severe limitations). In our view, the following are sensible criteria that the terms of a useful EDA should obey:

1. *Decomposition of a well-defined interaction energy.* An EDA should subdivide an intermolecular interaction energy calculated by a standard electronic structure method (e.g. user-chosen density functional) into physically interpretable contributions.
2. *Basis function independence.* EDA should not rely on a specific class of basis func-

tions, such as atomic orbitals (AO's), but rather should be applicable to any convenient basis including plane waves, wavelets, etc.

3. *Useful basis set limit.* At all relevant geometries, it should be possible to converge each energy term to a stable and physically meaningful complete basis set limit.
4. *Correct asymptotic behavior.* EDA terms must smoothly reproduce their known asymptotic behavior. For instance, polarization between neutral molecules with permanent dipoles has an asymptotic R^{-6} dependence.
5. *Valid quantum mechanical energies.* Intermediate EDA energies should be obtained from electronic states that obey Fermionic quantum mechanics.
6. *Continuous energies.* Intermediate energies and EDA components should be continuous functions of the nuclear coordinates if the overall intermolecular interaction energy is continuous.
7. *Computational feasibility.* The computational cost for evaluation of each term should not be significantly greater than the direct evaluation of the entire intermolecular interaction.
8. *Variationality.* To ensure validity in both weak and strong interaction regimes, the energy contributions should be defined as constrained variations relative to an unconstrained calculation.

Despite non-uniqueness, this list emphasizes that there is not complete freedom to model the contributions in **Figure 1**. Indeed, different, acceptable EDA models should yield qualitative agreement in the magnitude of their terms. We can in fact say that *a satisfactory understanding of intermolecular interactions will be reached when different, physically acceptable EDAs yield qualitatively similar results* for the contributions shown in **Figure 1**.

This article has several objectives in pushing towards that long-term goal. First is to describe the second generation of the variational EDA for DFT calculations that we have developed(10, 12, 13) based on absolutely localized molecular orbitals (ALMOs). It appears to be an acceptable EDA model in the sense that it formally meets the criteria laid out above. We note that some of these criteria may be cautiously loosened in practice to meet specific interpretation demands. We will briefly discuss the historical development of EDA, noting that a detailed blow-by-blow comparison up through 2015 is already available(14). There are also other worthwhile reviews(15, 16) that lay out success stories achieved with different EDAs, including the Block-Localized Wavefunction (BLW) approach(17) that is most closely related to the ALMO-EDA. A second goal is to describe some contributions to interpreting intermolecular interactions with this approach, with an emphasis on connecting such interpretations to experimental observables. The third goal is to discuss some applications of this EDA to validating and assessing representations of different terms contained in an advanced polarizable force field.

2. A BRIEF AND INCOMPLETE HISTORY OF EDA

The earliest popular EDA based on the supermolecular approach as captured in Eq. 1 is the Kitaura-Morokuma (KM)-EDA(18, 19). It partitions the mean-field Hartree-Fock (HF) interaction energy into electrostatic, exchange repulsion, polarization, charge transfer, and an unassigned mixed interaction components. In terms of the criteria listed above, the electrostatic and polarization terms are both defined using intermediate wavefunctions that are not fully antisymmetric, leading to potentially unphysical results. The KM-EDA also depends on an atomic orbital (AO) basis partitioning to separate polarization and charge

transfer.

EDA approaches for DFT calculations that are similar in spirit to KM-EDA were first proposed by Ziegler and Rauk (20, 21) and later generalized(22, 23). These EDAs divide a DFT interaction energy into electrostatic, Pauli, and orbital interaction contributions. As in KM-EDA, the electrostatic interaction is evaluated as the classical Coulomb interaction between isolated monomer charge distributions that are translated to their positions in the complex. The Pauli repulsion term in this method furthermore does not have a definite sign as it also includes the exchange-correlation (XC) functional contribution. Further extensions include the localized MO (LMO-EDA)(24) and generalized Kohn-Sham (GKS)-EDA(25). All the the above methods have been widely and successfully applied to a diverse range of chemical problems.(16, 26)

Meanwhile, a variationally well-defined partition of the orbital term into POL and CT contributions was achieved in the BLW-EDA(27, 28, 17), using fragment-blocking of the AO-to-MO coefficient matrix (29, 30, 31) to define an intermediate polarized state. The first version of the ALMO-EDA(32, 33, 34), from which the present work derives, was largely equivalent to the BLW-EDA, and introduced a perturbative partitioning of the CT term into forward and back-donation, as well as a charge-transfer analysis (CTA) of the electron flow. The same fragment-blocked MO coefficient matrix was also used to form a frozen orbital interaction energy using the MOs of isolated fragments. ALMO-EDA-I has been extended to excited states(35, 36), as well as to ground states using second-order Møller-Plesset perturbation theory (MP2).(37, 38, 39) While successful and quite widely used, BLW-EDA and ALMO-EDA-I lack useful basis set limits for the POL and CT terms,(40, 41, 42) and rely on the use of an AO basis. These challenges motivated the developments described in the following section.

Space limits preclude detailed discussion of other EDA approaches, but two must be mentioned. First, symmetry-adapted perturbation theory (SAPT)(43, 44) is a widely used approach that computes its own perturbative expansion of the interaction energy, rather than decomposing a DFT result. SAPT includes terms describing electrostatics, exchange, induction, dispersion, and various cross terms. The electrostatic contribution is equivalent to the quasi-classical electrostatic interaction. Exchange terms enter at all orders of the SAPT expansion as corrections to enforce proper antisymmetry. Induction contains both POL and CT contributions, which have proven challenging to separate.(45, 46, 42, 47) The combination of SAPT with DFT(44) is computationally quite efficient and acceptably accurate (48).

A second widely used approach for DFT calculations is the natural EDA (NEDA)(49, 50), which decomposes an interaction energy into contributions from electrostatics, polarization, charge transfer, a self-energy term, and a core term describing Pauli repulsion and exchange-correlation effects. This approach, however, has serious technical drawbacks. NEDA is not variational due to its dependence on the natural bond orbital (NBO)(51) procedure to identify a Lewis-like determinant for the polarized state. The CT contribution is defined as energy lowering from non-Lewis wavefunction components. While perhaps useful as a descriptor, CT from NEDA is unphysically large(52). As an example, NBO CT is on the order of 5 times larger than ALMO-EDA for the classic problem of the water dimer interaction energy(53, 47).

3. CONSTRAINED AND UNCONSTRAINED DFT ENERGIES

The overall objective of this section is to describe the definition and physical content of the terms in Eq. 2 within the DFT-based ALMO-EDA (10, 12, 13).

3.1. Orbitals and densities in Kohn-Sham DFT

Modern DFT(1) is exclusively performed within the Kohn-Sham construction, where a single determinant of occupied molecular orbitals (MOs), $\phi_i(\mathbf{r})$, exactly describes a set of fictitious non-interacting electrons. The key is that the density $\rho(\mathbf{r})$ associated with these fictitious electrons is the same as that of the interacting electrons, whose true wavefunction is extraordinarily complicated. Yet, KS-DFT is formally exact, and uses the MOs of the single determinant to generate the density, $\rho(\mathbf{r})$, as the diagonal elements of the one-particle density operator (1pdo) for the fictitious electrons ($\hat{\rho}$) in the position representation:

$$\hat{\rho}(\mathbf{r},\mathbf{r}') = \sum_i \phi_i(\mathbf{r})\phi_i^\star(\mathbf{r}') \qquad 3.$$

Variations of densities within KS-DFT is achieved by variation of orbitals, such that the KS-DFT energy is minimized.

There is a one-to-one relation between distinguishable KS orbitals, $\{\phi_i\}$ and the corresponding density operator, $\hat{\rho}$ for the fictitious electrons. Within EDA, we will apply constraints to the orbitals to prevent electron polarization and delocalization. These orbital constraints map directly to constraining the 1pdo and $\rho(\mathbf{r})$ as well, although we do not use that language in most of the review. The resulting EDA framework can be applied to any approximate density functional, including, in principle at least, the unknown exact density functional.

For later purposes, we establish some additional notation. Mathematically, the Pauli principle requires the Kohn-Sham 1pdo to be idempotent: $\hat{\rho}^2 = \hat{\rho}$. This ensures eigenvalues of 0 or 1, so that each KS orbital is either occupied or empty. Expressed in the orthonormal basis of occupied KS orbitals, the matrix representation of $\hat{\rho}$ is trivially $\mathbf{P}=\mathbf{1}$. In any other basis, such as atomic orbitals, $\mathbf{P} \neq \mathbf{1}$.

3.2. Isolated fragments and their preparation energy

The isolated fragment energies, E_F in Eq. 1 are evaluated at their equilibrium geometry in isolation. To bring them to their geometry in the complex whilst still isolated is associated with a "geometric distortion" energy, ΔE_{GD}. Typically the stronger the total molecular interaction, the greater the change in geometry of the monomers in the complex, and the larger ΔE_{GD} should become. If a fragment is a radical with partly occupied degenerate orbitals, such as $F^\bullet$, then there is also an electronic alignment necessary to make sure the frozen energy is well-defined (by orienting partly occupied degenerate orbitals consistently with the way they will polarize later). This procedure is accomplished by optimizing the fragment orbitals starting from the polarized complex (i.e. a polarize-then-depolarize procedure)(13).

3.3. Frozen energy and its further decomposition

The first intermediate energy of the complex, the frozen energy, E_{FRZ}, is so-named because it is the variational trial energy obtained by reusing the unmodified (i.e. frozen) orbitals of

the isolated fragments. The set of frozen MOs, $\boldsymbol{\phi}_{\rm FRZ}$ from a complex made from molecules A, B, C, ... is then $\boldsymbol{\phi}_{\rm FRZ} = \boldsymbol{\phi}_{\rm A} \oplus \boldsymbol{\phi}_{\rm B} \oplus \boldsymbol{\phi}_{\rm C} \oplus \ldots$. This frozen orbital constraint prevents energy lowering due to polarization and charge transfer. Physically, $\Delta E_{\rm FRZ}$ contains contributions from dispersion, Pauli repulsion, and permanent electrostatics(54):

$$\Delta E_{\rm FRZ} = \Delta E_{\rm DISP} + \Delta E^{\rm DF}_{\rm FRZ} = \Delta E_{\rm DISP} + \Delta E_{\rm PAULI} + \Delta E_{\rm ELEC} \qquad 4.$$

$\Delta E^{\rm DF}_{\rm FRZ}$ is a "dispersion-free" (DF) frozen energy change, to be defined shortly.

For fixed electron densities, electron correlation effects between electrons on non-overlapping fragments give rise to the attractive dispersion interaction. In the non-overlapping regime, the non-retarded inter-monomer dispersion is given by (9):

$$\Delta E_{\rm DISP}({\rm AB}) = -C_6({\rm AB}) R_{\rm AB}^{-6} - C_8({\rm AB}) R_{\rm AB}^{-8} - \ldots \qquad 5.$$

C_6(AB) coefficients arise from an integral of the products of the frequency-dependent polarizabilities of the monomers over imaginary frequencies. Just as electrostatic interactions can only be interpreted as multipole-multipole interactions in the non-overlapping regime, an EDA term that describes $\Delta E_{\rm DISP}$ is strictly dispersion only when fragments do not overlap. In the overlapping regime, $\Delta E_{\rm DISP}$ contains "dispersive" inter-fragment exchange-correlation effects that smoothly change into true dispersion as overlap decreases.

We separate $\Delta E_{\rm DISP}$ from other inter-fragment exchange-correlation effects(55) by using an auxiliary density functional that is dispersion-free (DF), $E^{\rm DF}_{\rm xc}$(54). Examples of DF functionals include Hartree-Fock (HF), the so-called dispersionless density functional (dlDF)(56), and revPBE(57). The preferred choice for $E^{\rm DF}_{\rm xc}$ varies with the choice of $E_{\rm xc}$: for example, HF is suitable for functionals with much exact exchange such as ωB97X-V(58), while dlDF or revPBE are more appropriate for semi-local functionals. $\Delta E_{\rm DISP}$ is then defined as the inter-fragment exchange-correlation energy captured by $E_{\rm xc}$ but *not* captured by $E^{\rm DF}_{\rm xc}$ (54).

Pauli repulsion is the dramatic increase in energy of a complex when overlapping fragments are compressed together. By antisymmetry, electrons of the same spin cannot occupy the same space. Physically, it is this volume exclusion effect that raises the energy (mainly through the kinetic energy component). In the basis of frozen orbitals, $\mathbf{P}_{\rm FRZ} = \mathbf{1}$ in the non-overlapping regime. As the occupied frozen orbitals of different fragments begin to overlap, with overlap matrix $\boldsymbol{\sigma}$, the frozen density matrix becomes $\mathbf{P}_{\rm FRZ} = \boldsymbol{\sigma}^{-1}$ to maintain idempotency. As $\boldsymbol{\sigma}$ deviates from $\mathbf{1}$, $\mathbf{P}_{\rm FRZ}$ progressively deforms from direct sum of fragment density matrices. These deformations ensure volume exclusion, and cause the energetic cost of Pauli repulsion.

How do we represent the densities of the fragments as the frozen density distorts to maintain idempotency? The simplest approach is to symmetrically orthogonalize the frozen fragment orbitals, $\boldsymbol{\phi}^{\rm orth}_{\rm FRZ} = \boldsymbol{\sigma}^{-1/2}\boldsymbol{\phi}_{\rm FRZ}$. A better orthonormal set of fragment orbitals can be obtained by minimizing the fragment energies, subject to orthonormality (54). This gives fragments that are as stable as possible subject to the volume exclusion (or kinetic energy pressure) exerted by their neighbors via the orthogonality constraint. The resulting orbitals yield deformed fragment densities that sum to the total density. An illustration of the deformations is given in **Figure 2(a)** for the $Cl^-\cdots HOH$ complex. Along the Cl···H hydrogen bond, Pauli repulsion leads to density depletion for each fragment in most of the intermolecular region and accumulation close to their own nuclei, with small enhancements on the other fragment that are orthogonalization tails.

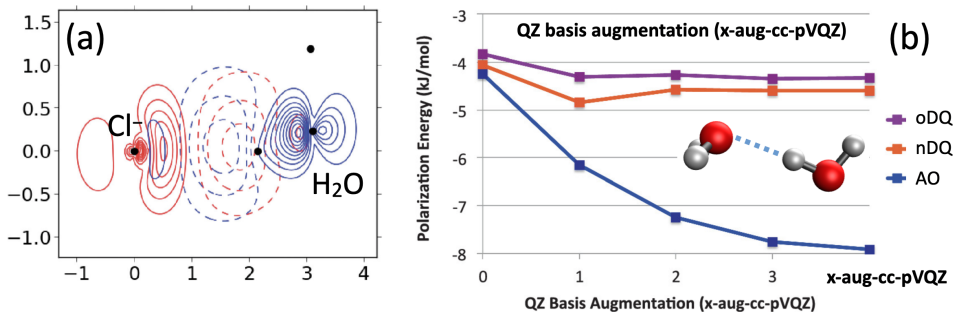

Figure 2

(a) An illustration of the z-integrated electron density distortions on chloride (red contours) and water (blue contours) associated with Pauli repulsion in the xy plane of the complex. Solid lines indicate density increases; dashed lines designate density decreases relative to the isolated fragment density; black dots indicate the positions of nuclei (adapted from ref. (54)); (b) Convergence of the polarization energy of the water dimer to a well defined basis set limit using a limited virtual space of dipole (D) and quadrupole (Q) FERFs, either without orthogonalization (nDQ) or with orthogonalization (oDQ). By contrast, using the AO-derived virtual orbitals of each fragment for polarization leads to increasing charge-transfer contamination of the polarization energy as the x-aug-cc-pVQZ basis approaches linear dependence through successive augmentation (increasing x). Adapted from ref. (41).

The frozen energy also contains the permanent electrostatic interactions of the fragments. In the non-overlapping limit, the electrostatic interaction between fragments A and B is rigorously:

$$\Delta E_{\mathrm{ELEC}}(\mathrm{AB}) = \iint \mathrm{d}\mathbf{r}_1 \mathrm{d}\mathbf{r}_2 \rho_{\mathrm{A}}^{\mathrm{tot}}(\mathbf{r}_1) r_{12}^{-1} \rho_{\mathrm{B}}^{\mathrm{tot}}(\mathbf{r}_2) \qquad 6.$$

where ρ^{tot} denotes a fragment charge density from both nuclei and electrons. When the fragments overlap, their densities have deformed as discussed above, and the quasi-classical expression using fixed fragment densities is no longer rigorously valid (because the fragment densities do not add up). Instead, the modified fragment densities defined by minimizing the kinetic energy pressure that add correctly to the frozen density can be used to evaluate the electrostatic interactions via Eq. 6 (54). Finally, $\Delta E_{\mathrm{PAULI}}$ is obtained by subtraction as the remainder of Eq. 4.

Use of the modified densities has the interesting implication that atomic charges and multipoles which reproduce the permanent electrostatics will *change* with inter-monomer separation when fragments overlap, even when the molecular geometry of the fragment is fixed. This is awkward from the viewpoint of force-field development (see e.g. **Section 6**) as well as being different from the convention used by almost all earlier EDAs. Nonetheless it is formally true. However, as a pragmatic alternative, one can also *define* the electrostatics to be the quasi-classical (QC) value, $\Delta E_{\mathrm{ELEC}}^{\mathrm{QC}}$, obtained by using *undistorted* isolated fragment densities, and then for consistency define the Pauli repulsion subtractively as $\Delta E_{\mathrm{FRZ}}^{\mathrm{DF}} - \Delta E_{\mathrm{ELEC}}^{\mathrm{QC}}$. In fact, this procedure will be employed in the examples discussed in **Sections 5.1** and **6**.

3.4. Intramolecular relaxation and the polarization energy

After E_{FRZ}, a constrained variational calculation is performed to evaluate the energy lowering due to polarization (POL). ΔE_{POL} describes the induced electrostatic interactions resulting from on-fragment density relaxation of each monomer due to the rest of the complex. In the non-overlapping regime, polarization is thus a response to the electric fields produced by other fragments' charge distributions. The strongest field at long distance is a dipolar field, if the molecule has a dipole moment, with higher order fields such as a quadrupolar field becoming important at shorter distances. In the overlapping regime, ΔE_{POL} also includes the effect of relaxing the Pauli repulsion associated with the frozen orbitals. For radicals, ΔE_{POL} additionally contains rehybridization (REHYB): the energy lowering due to reorganization of electron spin density on the radical species to "rehybridize" the odd-electron orbital in the presence of the environment (13).

These *intra-fragment* relaxations associated with the polarized intermediate state (with energy E_{POL}) must be accomplished with a constraint that still prevents *inter-fragment* charge transfer. To do this, the occupied frozen orbitals on each fragment, F, are allowed to mix with only *fragment-specific* virtual orbitals, rather than all virtual orbitals. A DFT calculation is then performed self-consistently with this constraint of a fragment-blocked MO coefficient matrix to yield E_{POL}. Such a calculation is commonly called SCF for molecular interactions (SCF-MI). Efficient algorithms are available for SCF-MI (29, 30, 59, 31). We call the resulting fragment-specific polarized orbitals "absolutely localized MOs" (ALMOs).

What should the fragment-specific virtual orbitals be? One simple choice that has been widely used is to take the virtual orbitals from the isolated fragment calculations, when performed in an atomic orbital (AO) basis. However, this is AO-specific which violates the EDA criterion of basis function independence. This approach also fails to have a useful basis set limit, because in a nearly overcomplete AO basis, each fragment has so many virtuals that E_{POL} becomes charge-transfer-contaminated,(40, 41, 42, 47) despite using fragment-specific virtual orbitals. This issue can largely be avoided in practice by using an adequate but not excessively large basis, such as def2-TZVPP (60).

Nonetheless, a better choice for the fragment-specific virtuals is a basis of fragment electric-field response functions (FERFs).(41) The FERFs allow each fragment to respond *exactly* to weak electric fields with the *fewest possible* virtual functions. For instance, the response of the H atom (1s orbital) to a weak uniform field along the z axis (e.g. which would be the leading effect due to a distant dipole on that axis) can be exactly represented using a single p_z virtual orbital. This result generalizes: 3 dipolar (D) virtual orbitals per occupied orbital exactly describe the response of a molecule to weak dipole fields. Similarly 5 quadrupolar (Q) FERFs per occupied orbital exactly describe the response of a molecule to weak quadrupolar fields, just as 5 d-like virtuals describe the response of a 1s orbital to each component of such a field.

Numerical tests establish that dipolar and quadrupolar FERF virtuals (FERF-DQ) is the lowest order that adequately reproduces polarization interactions as two molecules approach the overlapping regime(41). The FERF-DQ virtuals can be constructed from a large primitive basis of any type (e.g. AO's, or plane waves, etc), and the resulting SCF-MI energy has a meaningful complete basis set limit for E_{POL}. An example for the case of the water dimer is shown in **Figure 2(b)**. Successive augmentation of the large cc-pVQZ basis by more and more diffuse functions (increasing values of x) adds increasingly redundant functions to the basis, which does not alter the *overall* interaction energy significantly. However, using fragment AO-derived virtuals leads to unstable results for the *polarization*

energy because virtuals on one water molecule can mimic acceptor levels on the other molecule. In other words, ΔE_{POL} becomes charge-transfer contaminated. By contrast, the FERFs attain a useful basis set limit with or without orthogonalization (nonorthogonal FERFs are used by default in our implementation).

3.5. Intermolecular relaxation and the charge-transfer energy

The remaining energy lowering between the polarized state, E_{POL}, and the unconstrained DFT supermolecular energy, E_{FULL} is identified as due to *intermolecular* orbital mixing. We call this the charge-transfer (CT) contribution to connect with the language of donor-acceptor or dative interactions. For instance, in the water dimer, ΔE_{CT} corresponds mostly to the energy lowering from electron donation from an oxygen lone pair orbital, n_{O}, directed along the hydrogen bond, to an antibonding σ^*_{HO} orbital centered on the proton participating in the hydrogen bond. Note that ΔE_{CT} can also appropriately be termed the delocalization energy because it corresponds to stabilizing orbital interactions between different fragments, as opposed to the stabilizing intra-molecular relaxations contained in ΔE_{POL}(47).

The forward and back-donation contributions to ΔE_{CT} can be separated in a rigorous and well-defined fashion by writing $\Delta E_{\mathrm{CT}} = \mathrm{Tr}(\mathbf{F}_{\mathrm{eff}}\mathbf{\Theta})$, where $\mathbf{F}_{\mathrm{eff}}$ is an effective Fock operator(61) and $\mathbf{\Theta}$ is the generator of the unitary transformation connecting the polarized orbitals and density matrix to the fully relaxed solutions. Singular value decomposition of $\mathbf{\Theta}$ in the basis of occupied ALMOs and projected virtual ALMOs yields a description of the complementary occupied-virtual orbital pairs (COVPs) describing the charge transfer, with weights that describe their importance (33, 61). In favorable cases, only one pair dominates (i.e. all other weights are nearly zero), as shown in **Figure 3(a)** for the case of the water dimer, exhibiting the expected $n_{\mathrm{O}} \rightarrow \sigma^*_{\mathrm{HO}}$ character.

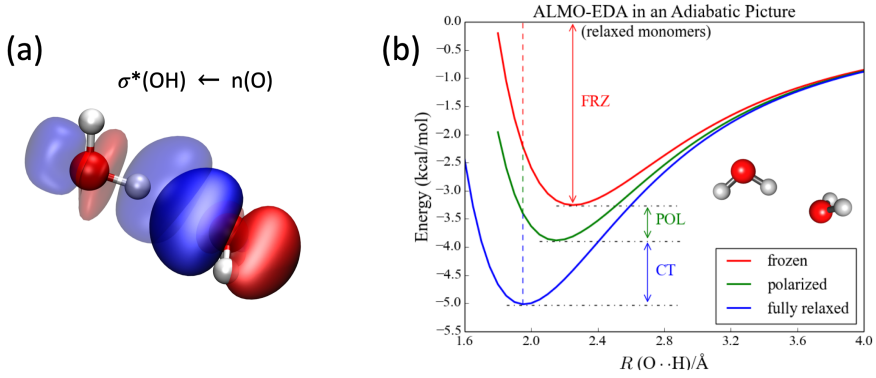

Figure 3

(a) Complementary occupied-virtual orbital pair (COVP) describing the $n_{\mathrm{O}} \rightarrow \sigma^*_{\mathrm{HO}}$ CT in the water dimer. The donor orbital is drawn bold; the acceptor orbital is pale. (b) Adiabatic ALMO-EDA scheme illustrated using the water dimer: the energy contributions are evaluated at the optimized geometry of each level of constraint (frozen, polarized, fully relaxed), as opposed to using the final geometry for all terms (the scheme represented by the dashed line). Adapted from Ref. 12.

4. VERTICAL AND ADIABATIC EDA

As discussed in **Section 1**, one challenge of EDA is the fact that the constrained intermediate energies and states, while quantum mechanically well-defined, are not directly observable. One can bridge the gap between physical observables and the physical driving forces for intermolecular interactions that are isolated in the EDA components by *computing those observables on each constrained potential energy surface*. The foundational property is the structure of the complex. As illustrated in **Figure 3(b)**, there is an optimized geometry on each surface ($E_{\rm FRZ}$, $E_{\rm POL}$, $E_{\rm FULL}$), as well as for each isolated fragment. The EDA form of the interaction energy given previously, Eq. 2, used only the energies at the final complex geometry, which, by analogy with spectroscopic transitions at a single geometry, should be viewed as a *vertical* EDA.

Using the optimized geometries on each constrained surface to define the energy increments yields an alternative *adiabatic* EDA (aEDA): (12)

$$\Delta E_{\rm INT} = \Delta E^{\rm ad}_{\rm FRZ} + \Delta E^{\rm ad}_{\rm POL} + \Delta E^{\rm ad}_{\rm CT} \qquad 7.$$

The *adiabatic* energy increments are defined as the energy difference between the optimal structures in each consecutive pair of states. For instance, denoting the optimized structures on the FRZ/POL surfaces as $\mathbf{R}_{\rm FRZ}/\mathbf{R}_{\rm POL}$, the adiabatic polarization energy, $\Delta E^{\rm ad}_{\rm POL}$ is

$$\Delta E^{\rm ad}_{\rm POL} = E_{\rm POL}(\mathbf{R}_{\rm POL}) - E_{\rm FRZ}(\mathbf{R}_{\rm FRZ}) \qquad 8.$$

To be computationally efficient, the aEDA requires analytic energy gradients for the intermediate energies, which was accomplished for $E_{\rm FRZ}$ (12). For $E_{\rm POL}$, analytic gradients are only available using the fragment AO-derived virtuals at present (62, 12) (the implementation with FERF virtuals is non-trivial).

As will be illustrated in **Section 5**, the aEDA approach very nicely enables one to identify whether shifts in observables such as structure, vibrational frequencies, etc. are associated with FRZ, POL, CT, or some admixture of each. If CT controls observable changes, it is possible to further explore the relative roles of forward and back-donation in influencing the observables using the *variational forward-backward* (VFB) analysis (63). The VFB approach employs two additional constrained intermediate states one of which includes only forward donation plus polarization (denoted as CTf), and the other only backward donation and polarization (CTb). With the aid of a generalized SCF-MI implementation (41, 63), these two "one-way" CT states are variationally optimized, from which one can obtain estimates for the strength of forward and backward CT energies:

$$\Delta E_{\rm CTf/b} = E_{\rm CTf/b} - E_{\rm POL} \qquad 9.$$

As the analytical nuclear forces associated with the CTf/CTb states can be easily obtained, we augmented aEDA with the VFB scheme so that the molecular property changes arising from forward and back donations can be evaluated individually (63).

5. CHEMICAL EXAMPLES

5.1. Red- vs. Blue-Shifting Hydrogen Bonds

Hydrogen bonds (HB, denoted as X−H$\cdots$Y) constitute one of the most common motifs of intermolecular interactions and they play a crucial role in chemistry and molecular biology.

Using the ALMO-EDA to probe an HB, one would typically conclude that the stabilization effect is dominated by permanent electrostatics accompanied by notable contributions from polarization and charge transfer (53, 10, 13). This contrasts with either the pure electrostatic view of the σ-hole model (5, 6) or the pure donor-acceptor interaction view coming from NBO theory (7, 8). The balanced role of permanent electrostatics (encompassed in the frozen interaction) and orbital interaction in the water dimer, a prototypical HB, can be seen in **Figure 3(b)**.

One common spectroscopic signature of HB is the red shift in X−H stretch frequency (ν_{XH}) relative to that in a free XH molecule. Employing the adiabatic ALMO-EDA, we have revealed that for most common HB complexes the red shift in ν_{XH}, as well as the accompanied elongation of the X−H bond, mainly results from CT despite the prominent role of electrostatics in energetic stabilization (64, 12). The results for three prototypical HB complexes, the H_2O dimer, HF dimer, and the $H_2O\cdots Cl^-$ complex are shown in Table 1.

Table 1 X–H bond lengths (Å) and XH stretch frequencies (cm^{-1}) for H-bonding complexes X–H$\cdots$Y calculated at the isolated fragment, frozen, polarized, and fully relaxed levels with ωB97X-V/def2-TZVPPD. The data are adapted from Ref. 47.

	H_2O dimer		HF dimer[a]		$H_2O\cdot\cdot Cl^-$	
	r_{OH}	ν_{OH}	r_{FH}	ν_{FH}	r_{OH}	ν_{OH}
Isolated[b]	0.960	3863	0.921	4128	0.960	3863
FRZ	0.961	3861	0.922	4120	0.962	3866
POL	0.962	3853	0.923	4095	0.968	3803
Full	0.967	3754	0.928	3981	0.987	3406

[a]In order to decouple the two FH modes in the HF dimer, the non-H-bonded hydrogen is deuterated.
[b]For H_2O, the frequency of the symmetric OH stretch mode is reported.

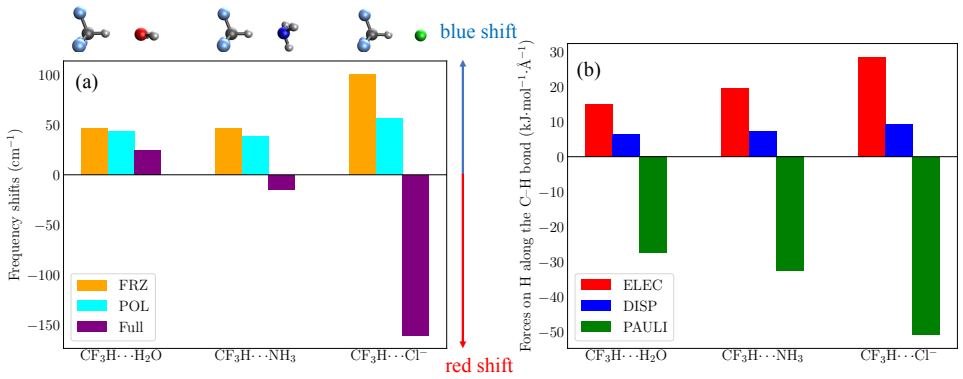

Figure 4

(a) Shifts in X−H stretch frequency (in cm^{-1}) evaluated on the FRZ, POL, and fully relaxed surfaces for the $CF_3H\cdots Y$ complexes (Y = H_2O, NH_3, and Cl^-); (b) Decomposition of intermolecular forces exerted on the H atom along the C−H bond direction at the minimum-energy structures on the FRZ surface, where positive/negative forces stretch/compress the C−H bond (adapted from Ref. 65). All calculations were performed at the ωB97X-V/def2-TZVPPD level of theory.

However, there are exceptions where the X−H bond is contracted and ν_{XH} blue-shifted,

which are called "improper, blue-shifting" hydrogen bonds (66, 67). The origin of blue-shifting HB has become a subject of debate since the conclusion varies with the choice of computational analysis tools. As a result, the origin of blue-shifting HB has ever been attributed to almost every single component of the interaction (permanent electrostatics, charge transfer, dispersion, etc.) and thus still remains elusive.

To elucidate the origin of blue-shifting HB, we investigated complexes of fluoroform (CF_3H) with three Lewis bases of distinct electron-donating abilities (H_2O, NH_3, and Cl^-) using the adiabatic ALMO-EDA (65). We demonstrated that all three complexes are most blue-shifted on the FRZ surface (**Figure 4(a)**), ruling out the possibility of POL or CT being the source of blue shifts. Since the blue shift in ν_{XH} is always associated with shortening of the C−H bond in these complexes, we further decomposed the intermolecular forces exerted on the H atom in CF_3H along the C−H bond direction at the equilibrium structures on the FRZ surface. **Figure 4(b)** shows that among the three components of frozen interaction, only Pauli repulsion compresses the C−H bond (inducing blue shift) while both permanent electrostatics and dispersion interaction lengthen the C−H bond (inducing red shift). Our analysis thus unambiguously identified Pauli repulsion as the only blue-shifting force in the bonding regime. The final shift in ν_{XH} is also determined by the strength of CT which is always a red-shifting effect: relatively weak CT turns out to be a prerequisite for blue-shifting HB since otherwise the blue-shifting frozen interaction will be overcome, as in $CF_3H\cdots NH_3$ and $CF_3H\cdots Cl^-$.

With these HB complexes, we have shown that the combination of vertical and adiabatic variational ALMO-EDA schemes can offer a "panoramic" view of intermolecular interactions, ranging from identifying major components for energetic stabilization to revealing origins of shifts in observable properties. One can use the same protocol to explore many intriguing interaction motifs, such as halogen/pnicogen/tetrel bonds, cation–π/anion–π interactions, etc., facilitating the understanding of their physical nature.

5.2. Coordination Chemistry of Isoelectronic π-Acidic Ligands: N_2, CO, and BF

The pentaamine(dinitrogen)ruthenium(II) complex is a classic inorganic compound, as it was the first reported coordinated dinitrogen complex with an experimentally measured red shift in the N−N stretching frequency ($\sim$190 cm^{-1}) (68). N_2, like many other π-acidic ligands, is stabilized by bi-directional charge transfer involving two different types of orbital interactions according to the Dewar–Chatt–Duncanson model (69, 70): σ forward donation and π back-donation, which are revealed by the COVPs shown in **Figures 5(a)** and **5(b)**, respectively. Carbon monoxide (CO), isoelectronic with N_2, is the most prominent ligand of this type and governs a wide range of organometallic compounds. The red shift in carbonyl complexes typically falls in the range of 0–300 cm^{-1}(71) with the exception of nonclassical metal carbonyls (72, 73) where ν_{CO} is blue-shifted. The third isoelectronic ligand, BF, was long predicted to be an excellent ligand but it had not been prepared in experiments until recently (74). Along this isoelectronic series, the π^* orbital becomes more polarized toward the coordinating atom from N_2, CO to BF, rendering the latter two more susceptible to back-donation due to their better overlap with the metal d orbitals. The red shift in the stretching frequency of the ligand is often used as an indicator for the strength of back-donation as the population of the π^* orbitals reduces the bond order. In addition, the dipole moment increases in the order of $N_2 < CO < BF$, with the negative pole counter-intuitively located on the more electropositive C/B atom.

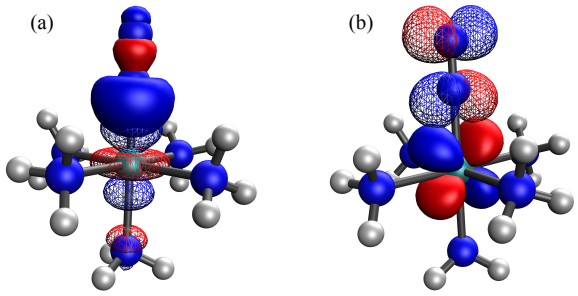

Figure 5

Key COVPs illustrating the σ- and π-type donations in $[Ru(NH_3)_5(N_2)]^{2+}$: (a) σ forward donation, (b) π backward donation. All calculations were performed at the B3LYP/def2-TZVPP level of theory; donor orbitals are in solid colors and the acceptor orbitals are meshed.

Recently we provided a systematic study of octahedral transition metal complexes with these three isoelectronic ligands (N_2, CO, and BF) coordinated to a $[Ru(II)(NH_3)_5]^{2+}$ moiety (63). The shifts in their stretching frequencies ($\Delta\nu$(X-Y)) follow a counter-intuitive trend with a red shift of 150 cm^{-1} for N_2, a smaller red shift of 102 cm^{-1} for CO, and a significant blue shift of 123 cm^{-1} for BF. Our comprehensive analysis based on ALMO-EDA shed light on the bonding and IR frequency shifts in these complexes.

The vertical EDA results of the three complexes (**Table 2**, upper) reveal that CT is the dominant stabilizing factor in all three complexes since the significant Pauli repulsion cannot be overcome by other attractive forces (ELEC, POL, and DISP) alone. The total interaction energy (ΔE_{INT}) follows the same trend as ΔE_{CT}: N_2 < CO < BF. The VFB decomposition of the CT energy reveals that N_2 is both a weaker σ-donor and a weaker π-acceptor than the more polar CO and BF ligands. This is because the increase in bond polarity (N_2 < CO < BF) in this isoelectronic series increases the charge density on the coordinating atom, reduces the HOMO-LUMO gap, and yields more polarized π^* orbitals, thereby facilitating both forward and backward donations. Interestingly, the relative strength of forward donation increases more rapidly than backward donation with the ligand polarity, as indicated by the increased CTf/CTb ratio from N_2 to BF.

The adiabatic EDA results (**Table 2**, lower) for the complex geometries show that all three ligands only weakly coordinate without CT, with Ru−X distances over 2.6 Å on the POL surface. Both CTf and CTb contribute to pulling the ligand considerably closer (∼0.3 Å). The relative effects of CTf and CTb on the metal-ligand distance show good agreement with the trend in their CTf/CTb ratios as well as excellent additivity.

The trend in $\Delta\nu$(X-Y), on the other hand, is not consistent with the relative strength of CTb along the series (see **Table 2**). Nonetheless, this trend can be explained by the decomposition of the frequency shift. The CT-forbidden frequencies (at the POL level) are blue-shifted in all three complexes, and the shifts are particularly large for the polar ligands CO and BF due to the molecular Stark effect. This effect originates from the fact that the dipole moment of these diatomic molecules increases when the X−Y bond is contracted, and thus it leads to shortened and blue-shifted X−Y to achieve more favorable electrostatic interactions when CT is absent. It is important to note that the orientation of the X-Y dipole determines the direction of this effect, e.g., in a κ-*O* bound metal carbonyl, the molecular

Table 2 Upper table: vertical ALMO-EDA results (in kJ/mol) at the B3LYP/def2-TZVPP level of theory for $[Ru(II)(NH_3)_5(XY)]^{2+}$ (XY = N_2, CO, and BF) and the $\Delta E_{CTf}/\Delta E_{CTb}$ ratio; Lower table: metal-ligand distance [r(M−X), in Å] and shifts in the stretch frequency of the diatomic ligand [$\Delta\nu$(X−Y), in cm^{-1}] obtained from adiabatic ALMO-EDA calculations

Ligand	ΔE_{FRZ}	ΔE_{POL}	ΔE_{CTf}	ΔE_{CTb}	ΔE_{CT}	ΔE_{INT}	ratio
N_2	160.4	−70.1.	−95.0	−99.5	−212.6	−122.4	1.0
CO	283.2	−119.6	−190.0	−155.8	−392.8	−229.2	1.2
BF	317.1	−171.0	−284.8	−130.0	−477.2	−331.1	2.2

	r(M−X)				$\Delta\nu$(X−Y)			
	POL	CTf	CTb	Full	POL	CTf	CTb	Full
N_2	2.625	2.308	2.318	1.951	11	25	−39	−150
CO	2.605	2.219	2.329	1.860	74	109	−5	−102
BF	2.690	2.165	2.379	1.871	143	208	108	123

Stark effect induces a red shift in $\Delta\nu$(X−Y) (63). The VFB analysis on ν(X−Y) further revealed the other key contributor to the final frequency shift — the well-known red-shifting effect of π back-donation. In contrast to the Stark effect, this effect is always red-shifting regardless of ligand orientation. In the full complexes, the effects of POL and CTf on $\Delta\nu$(X−Y) are mainly "geometric", i.e., they enhance both the blue-shifting Stark effect and the red-shifting back-donation through shortening the metal-ligand distance r(M−X). Interestingly, in the BF complex the blue-shifting Stark effect increases more rapidly than the red-shifting back-donation with the shortening of r(M−X), while the opposite occurs in the carbonyl and dinitrogen complexes (63).

To summarize, this counterintuitive trend in ν(X−Y) shifts along the isoelectronic series N_2, CO, and BF can be explained by two competing factors: (i) increase in the X-Y dipole moment that enhances the blue-shifting molecular Stark effect; (ii) increasingly polarized π^* orbitals along the series that facilitate the red-shifting back-donation. This example shows that shifts in ν(X−Y) alone are *not* a reliable metric for the strength of π back-donation.

5.3. Adducts between Pyridine and Aromatic Radical Cations

ALMO-EDA can probe intermolecular interactions between radicals and closed-shell molecules (34, 13), which play important roles in atmospheric and interstellar chemistry. As an example, we apply the second-generation ALMO-EDA with unrestricted orbitals (uALMO-EDA) to the benzene$^{+\bullet}$–pyridine (Bz$^{+\bullet}$–Py) and naphthalene$^{+\bullet}$–pyridine (Naph$^{+\bullet}$–Py) complexes (13), which originate from nucleophilic attack of neutral pyridine to aromatic radical cations formed in ionizing environments (75). The resulting distonic (i.e. the charge is on Py; the odd electron on the aromatic) adducts are remarkable. They have typical C−N bond lengths, but the binding energy is far weaker than a single bond.

The uALMO-EDA results at the equilibrium structures are shown in **Table 3**. While the equilibrium C−N distances of these two complexes are almost identical (1.53 Å), their total binding energies (BIND) differ substantially by over 15 kcal/mol, which mainly stems from the difference in the PAULI term (19.6 kcal/mol) according to the EDA results. In addition to that, the geometry distortion (GD) term as the energy cost in the preparation for the complexation process also contributes 4.5 kcal/mol to the difference in binding energy.

Despite being less strongly bound, the POL contribution is markedly more favorable

Table 3 Vertical uALMO-EDA results (in kcal/mol) for the $Bz^{+\bullet}$–Py and $Naph^{+\bullet}$–Py complexes at equilibrium geometries calculated at the ωB97M-V/def2-TZVPD level of theory (adapted from Ref. 13).

	$Bz^{+\bullet}$–Py	$Naph^{+\bullet}$–Py	$\Delta\Delta E^{a}$
ELEC	-75.2	-77.5	-2.2
PAULI	245.5	265.1	19.6
DISP	-17.6	-18.8	-1.2
POL[b]	-124.8	-131.2	-6.4
CT	-91.6	-90.3	1.3
TOTAL	-63.7	-52.6	11.1
REHYB	-8.3	-14.9	-6.6
EL_POL	-116.5	-116.3	0.2
GD	23.3	27.8	4.5
BIND[c]	-40.4	-24.8	15.6

[a] $\Delta\Delta E$ refers to the difference between the EDA results of these two complexes.
[b] POL = REHYB + EL_POL; [c] BIND = GD + INT

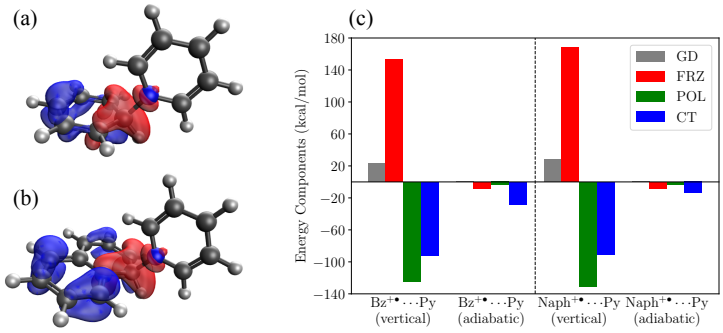

Figure 6

(a)(b) Reorganization of the electron spin density ($\rho_\alpha - \rho_\beta$) in $Bz^{+\bullet}$–Py and $Naph^{+\bullet}$–Py upon the rehybridization step (relative to the FRZ state, isovalue = 0.001 a.u.). Red color indicates regions with increased ρ_α or decreased ρ_β while blue indicates the opposite; (c) Comparison between the vertical and adiabatic ALMO-EDA results for $Bz^{+\bullet}$–Py and $Naph^{+\bullet}$–Py. Adapted from Ref. 13.

in the $Naph^{+\bullet}$–Py complex. Under the uALMO-EDA framework, the polarization energy in a radical-molecule complex comprises two distinct contributions (13): (i) rehybridization (REHYB), which is the energy lowering due to reorganization of electron spin density on the radical species that effectively "rehybridizes" the odd-electron orbital; (ii) electrical polarization (EL_POL), which corresponds to the mixing of occupied orbitals with polarization-specific virtuals defined by FERFs. Using uALMO-EDA we demonstrated that the stronger polarization in $Naph^{+\bullet}$–Py almost entirely arises from its more significant REHYB term(13): the energy lowering associated with localization of the radical orbital. This effect is visualized in **Figures 6(a)** and **6(b)**, where spin density is depleted from the aromatic system and accumulated around the C atom making the dative bond with Py.

While vertical EDA results (**Table 3**) attribute the stronger binding of the $Bz^{+\bullet}$–Py complex to its less unfavorable Pauli repulsion, this is not the *driving force* behind stronger binding. In addition, POL is larger than CT in both systems, which is counterintuitive for

this dative Lewis base–radical cation interaction. For strong donor-acceptor complexes with short intermolecular distances, adiabatic ALMO-EDA typically provides a complementary view that is in sharp contrast to that given by vertical EDA, as shown in **Figure 6(c)**. The FRZ, POL, and CT components obtained from adiabatic EDA are all attractive and are smaller in magnitude than those produced by vertical EDA. The driving force for the stronger binding of the $Bz^{+\bullet}$–Py complex is instead attributed to its more favorable CT, consistent with the higher ionization potential of benzene versus naphthalene.

6. CONNECTIONS TO FORCE FIELD DEVELOPMENT

6.1. Assessment of Advanced Force Fields using EDA

Molecular modeling has historically relied on the pairwise additive approximation to represent the potential energy surface of molecules.(76) We define advanced force fields as those that move beyond the pairwise approximation by incorporating many-body interactions as well(77), with the following general functional form

$$U = U_{\mathrm{Val}} + U_{\mathrm{elec}} + U_{\mathrm{Pauli}} + U_{\mathrm{disp}} + U_{\mathrm{CP}} + U_{\mathrm{pol}} + U_{\mathrm{CT}} \qquad 10.$$

The first term, U_{Val}, defines the valence description for molecules, and thus classifies the force field as capable of describing reactive chemistry or restricted to non-reactive applications such as predicting conformational equilibria or phase behavior. We focus on the non-reactive case in this review for which U_{Val} is composed of harmonic bond and angle terms, and anharmonic torsions.

The remaining non-bonded terms can be mapped to the terms in the EDA developed in previous sections. For example, the permanent electrostatics term U_{elec} can be connected to the (quasi-classical) ΔE_{ELEC} in EDA as they both describe Coulombic interactions between fragment charge distributions. Most advanced potential energy surfaces retain terms in the expansion beyond the monopole, which better accounts for short-ranged anisotropic hydrogen-bonding in particular. The U_{Pauli} and U_{disp} terms map to their counterparts in our EDA. In force fields they are typically combined within different representations such as the 12-6 Lennard-Jones potential that describes noble gases reasonably well but yields a too repulsive wall in practice for molecules(78). The buffered 14-7 functional form(79) used in the AMOEBA potential (80, 81, 82, 83) accounts for a less stiff repulsive wall and the expansion of dispersion to higher order terms.

The most popular class of many-body potentials are those that include the polarization term, U_{pol} (84, 85, 86, 87, 80, 88, 89, 90, 91). Three main approaches have emerged to calculating polarization in empirical force fields. The fluctuating charge and Drude oscillator approaches have been reviewed in detail elsewhere (92, 93) and they can be viewed as functional form extensions to atom-centered charge models to accommodate polarization. Instead we have been developing the induced dipole model where the natural link to a Taylor expansion of the energy in the field $\mathbf{E}$ motivates the permanent multipole expansion and multipole polarizabilities (94, 95). It also has an obvious connection to the FERF polarization model in ALMO-EDA.

The charge-penetration (U_{CP}) and charge-transfer (U_{CT}) terms are unmistakably more quantum in nature and/or many-body in character, and tend to be more short-ranged and thus difficult to model due to interference among all non-bonded and bonded interactions. While CT has been introduced in previous sections, CP describes the additional gain in attractiveness of electrostatics in the overlapping regime stemming from the spatial extent of

fragment electron densities. Since some polarizable force fields neglect U_{CP} and U_{CT}(96, 81), and fixed charge models ignore many-body interactions by design, these force fields must rely on a cancellation of errors through their take up into the remaining molecular interaction terms such as U_{Pauli}, U_{elec}, and U_{pol} if present. Despite this drawback, pairwise additive force fields continue to be successfully developed and applied by taking advantage of fitting to a combination of high-quality experimental data and first-principles calculations to realize effective Hamiltonians for missing interactions, using sophisticated optimization approaches such as the ForceBalance method.(97, 98)

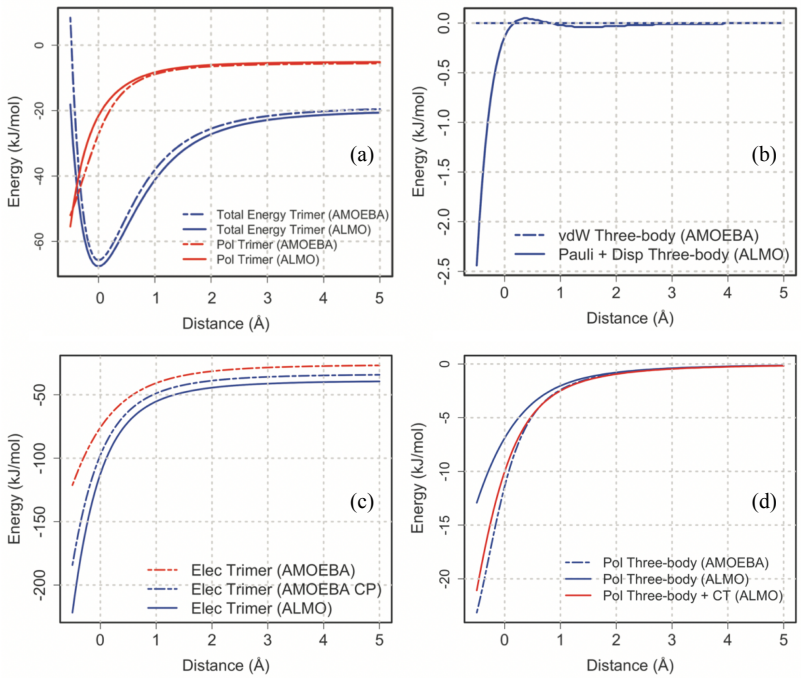

Figure 7

Comparison of various energy components in AMOEBA against the ALMO-EDA counterparts for the H_2O trimer: (a) total interaction energy and polarization energy given by AMOEBA and ALMO-EDA with ωB97X-V/def2-QZVPPD; (b) 3-body van der Waals (which is zero in AMOEBA) vs. 3-body PAULI+DISP in ALMO-EDA; (c) AMOEBA permanent electrostatics with and without charge penetration compared to ALMO-EDA; (d) 3-body polarization of AMOEBA compared to 3-body POL and 3-body POL+CT in ALMO-EDA. Adapted from Ref. 99.

The underlying hypothesis of advanced potential energy surfaces is that the many-body expansion is valid(100, 86, 101, 102), and hence ab initio generated cluster data should be sufficient without need for experimental data. Furthermore, the decomposition of cluster data with an EDA can diagnose successes and limitations of the many-body force fields and aid their modeling of additional interactions such as CP and CT. To illustrate, we have evaluated the accuracy of the classical AMOEBA03 water model(80) for representing many-body interactions such as polarization, charge transfer, and Pauli repulsion and dispersion, through comparison against the DFT-based ALMO-EDA for the water trimer (**Figure 7**), as well as for a variety of ion-water systems(103, 99, 104, 105). The original AMOEBA03

water model was found to underbind the water trimer throughout the distance perturbation of pulling one of the waters out of its equilibrium position (**Figure 7a**). The comparison against ALMO-EDA found that 3-body dispersion was largely negligible (**Figure 7b**) and could not account for this error, a reassuring assumption of its neglect in classical force fields relevant to the condensed phase. Instead errors in the AMOEBA03 water model arose first through permanent electrostatics, which is severely underestimated due to neglect of CP(106, 107, 108) (**Figure 7c**), and second because the 3-body polarization disagrees with the ALMO-EDA result (**Figure 7d**). Some bright spots to note are AMOEBA03's excellent agreement with ALMO-EDA on 2-body polarization (likely stemming from its tight fit to the water dimer) and its valiant attempt to incorporate missing CT effects through its polarization term (**Figure 7d**) and the missing effects of CP through softening its van der Waals wall(103). Overall, the error cancellation attempts that are crucial to the accuracy of the AMOEBA03 and other polarizable models could be replaced by efforts to represent all non-bonded terms explicitly with the aid of variational ALMO-EDA, with the potential for improved accuracy.

6.2. Development of an Advanced Force Field for Water using EDA

Our recent (many-body) MB-UCB force field for water(102) explicitly accounts for the decomposed molecular interactions commensurate with the variational ALMO-EDA, incorporates anisotropic polarization, charge penetration, and charge transfer, and makes force field design choices that reduce the computational expense while remaining accurate. While all properly designed EDA approaches agree in the asymptotic region for intermolecular interactions, they are non-unique at or near equilibrium and into the compressed region when electron densities of the molecular fragments overlap. Our view is that a force field that reproduces the piecewise energy decomposition of any particular EDA scheme, and in turn shows that it is transferable to describe a larger or more complex system or phase, is an important way to fully validate any particular EDA approach.

The ALMO-EDA diagnosis of the water trimer led to our first introduced improvement to the AMOEBA water force field by developing an anisotropic polarizable model as the primary approach to improve the many-body polarization.(91) We found that the accounting of anisotropy for a single water molecule (which therefore does not rely on EDA for fitting) demonstrably improved the description of the many-body polarization energy in all cases examined across a wide range of water cluster data as well as ambient properties such as liquid structure. Use of anisotropic polarization yielded good accuracy with a lower-order atomic multipole model for permanent electrostatics (truncated at dipoles instead of quadrupoles). This is a benefit due to the redundancy in multipole representation (109). When combined with the CP model of Piquemal and co-workers(110), there was no longer a need to capture this missing effect through the van der Waals term(102). Similarly, our incorporation of a simple CT model, identical to the induced dipole polarization term except for a different damping function that makes it more short-ranged than polarization, allowed us to separate U_{CT} from polarization to better match its ALMO-EDA counterpart through cluster data up through pentamers (102).

Figure 8 shows that very high accuracy is obtained when the MB-UCB water model is validated against experimental data for radial distribution functions of the liquid phase and the temperature dependence of thermodynamic and transport water properties, despite the absence of condensed phase data in training. MB-UCB is comparable in performance to

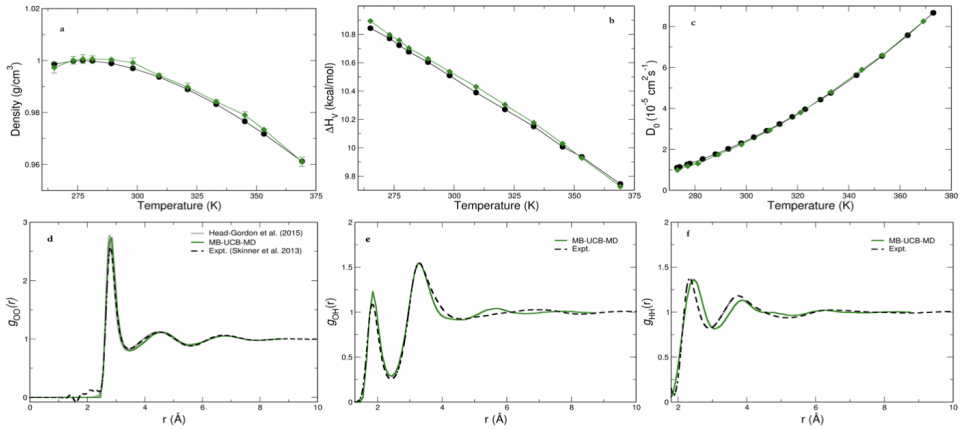

Figure 8

Thermodynamic, transport, and structural properties for MB-UCB (green) vs. experiment (black): (a) density, (b) diffusion coefficients corrected for finite size effects, (c) heat of vaporization, (d-f) O-O, O-H and H-H radial distribution functions for bulk water. For $g_{OO}(r)$ the gray curves correspond to a family of allowed rdfs that remove the unphysical density at very low r and all conform to the isothermal compressibility(111). Reproduced with permission from Ref. 102

the highly accurate MB-pol model(112, 113), but is less expensive and more transferable by eliminating the need to represent short-ranged QM interactions through large parameter fits to high-order polynomials. This illustrates the value of the EDA-guided piecewise parameterization approach to rational force field design.

7. CONCLUSIONS AND FUTURE ISSUES

The development of an EDA whose terms are mathematically well-defined with a clear mapping to physically and chemically useful contributions is an important problem. Such an EDA can be applied with reasonable confidence to gain insight into problems where the nature of an intermolecular interaction is not immediately clear. This article has described the development of the second generation of the absolutely localized molecular orbital EDA (ALMO-EDA), which appears to meet this objective. A particular strength of ALMO-EDA is the ability to connect the component physical contributions to shifts in experimental observables beyond the interaction energy itself, via the adiabatic EDA formalism. A series of chemical examples illustrates these capabilities to shed light on interactions ranging from weak hydrogen bonds, to much stronger metal-ligand interactions, and complexes between a Lewis base, pyridine, and aromatic radical cations. Additionally, if the quantum mechanical energy and forces can be decomposed based on sound chemical principles, a position long formulated within classical force fields which are also piecewise decomposable by design, non-bonded interactions can be better quantified. Hence, there is a valuable synergy between EDA development and its application to the development of advanced potential energy surfaces.

There are interesting extensions of the ALMO-EDA that space limits have prevented us from describing. These include the generalization from ground state to excited state

exciplexes and excimers (35, 36), and the development of an EDA-based fingerprint to characterize single chemical bonds (114, 115). We have also limited our scope to describing DFT-based EDA, although there has been progress in developing an analogous ALMO-EDA to treat intermolecular interactions described by second-order Møller-Plesset perturbation theory (37, 38, 39). There are also a range of opportunities for further development of the ALMO-EDA approach. One topic that is underway is generalization to include energy changes upon complex formation in continuum solvent models (116). The question of appropriate generalization to intramolecular interactions is also far from fully resolved. One might also consider the possibility of developing EDA approaches to understand other types of chemically important property shifts upon complexation, such as magnetic properties. Most importantly, there are numerous interesting potential applications across chemistry, biology, and catalysis where additional insight may be gained from use of state-of-the-art EDA such as described here.

DISCLOSURE STATEMENT

M. Head-Gordon is a part-owner of Q-Chem Inc., which distributes software that includes the EDA tools discussed in this review.

ACKNOWLEDGMENTS

We are grateful to the National Science Foundation for funding the work described here for long enough to make meaningful progress, through Grants CHE-1363342, CHE-1665315, and CHE-1955643.

LITERATURE CITED

1. Mardirossian N, Head-Gordon M. 2017. Thirty years of density functional theory in computational chemistry: an overview and extensive assessment of 200 density functionals. *Mol. Phys.* 115:2315–2372
2. Goerigk L, Hansen A, Bauer CA, Ehrlich S, Najibi A, Grimme S. 2017. A look at the density functional theory zoo with the advanced gmtkn55 database for general main group thermochemistry, kinetics and noncovalent interactions. *Phys. Chem. Chem. Phys.* 19:32184–32215
3. Grimme S, Antony J, Ehrlich S, Krieg H. 2010. A consistent and accurate ab initio parametrization of density functional dispersion correction (DFT-D) for the 94 elements H-Pu. *J. Chem. Phys.* 132:154104
4. Vydrov OA, Van Voorhis T. 2010. Nonlocal van der Waals density functional: The simpler the better. *J. Chem. Phys.* 133:244103
5. Murray JS, Riley KE, Politzer P, Clark T. 2010. Directional weak intermolecular interactions: σ-hole bonding. *Aust. J. Chem.* 63:1598–1607
6. Murray JS, Politzer P. 2017. Molecular electrostatic potentials and noncovalent interactions. *WIREs: Comput. Mol. Sci.* 7:e1326
7. Weinhold F, Klein RA. 2012. What is a hydrogen bond? mutually consistent theoretical and experimental criteria for characterizing h-bonding interactions. *Mol. Phys.* 110:565–579
8. Weinhold F, Klein RA. 2014. What is a hydrogen bond? resonance covalency in the supramolecular domain. *Chem. Educ. Res. Pract.* 15:276–285
9. Stone AJ. 2013. *The Theory of Intermolecular Forces*. Oxford: Oxford University Press, 2nd ed.
10. Horn PR, Mao Y, Head-Gordon M. 2016. Probing non-covalent interactions with a second

generation energy decomposition analysis using absolutely localized molecular orbitals. *Phys. Chem. Chem. Phys.* 18:23067–23079
11. Andrés J, Ayers PW, Boto RA, Carbó-Dorca R, Chermette H, et al. 2019. Nine questions on energy decomposition analysis. *J. Comput. Chem.* 40:2248–2283
12. Mao Y, Horn PR, Head-Gordon M. 2017. Energy decomposition analysis in an adiabatic picture. *Phys. Chem. Chem. Phys.* 19:5944–5958
13. Mao Y, Levine DS, Loipersberger M, Horn PR, Head-Gordon M. 2020. Probing radical–molecule interactions with a second generation energy decomposition analysis of dft calculations using absolutely localized molecular orbitals. *Phys. Chem. Chem. Phys.* 22:12867–12885
14. Phipps MJS, Fox T, Tautermann CS, Skylaris CK. 2015. Energy decomposition analysis approaches and their evaluation on prototypical protein-drug interaction patterns. *Chem. Soc. Rev.* 44:3177–3211
15. Pastorczak E, Corminboeuf C. 2017. Perspective: Found in translation: Quantum chemical tools for grasping non-covalent interactions. *J. Chem. Phys.* 146:120901
16. Zhao L, von Hopffgarten M, Andrada DM, Frenking G. 2018. Energy decomposition analysis. *WIREs: Comput. Mol. Sci.* 8:e1345
17. Mo Y, Bao P, Gao J. 2011. Energy decomposition analysis based on a block-localized wavefunction and multistate density functional theory. *Phys. Chem. Chem. Phys.* 13:6760–6775
18. Kitaura K, Morokuma K. 1976. A New Energy Decomposition Scheme for Molecular Interactions within the Hartree-Fock Approximation. *Int. J. Quantum Chem.* 10:325–340
19. Morokuma K. 1977. Why Do Molecules Interact? The Origin of Electron Donor-Acceptor Complexes, Hydrogen Bonding and Proton Affinity. *Acc. Chem. Res.* 10:294–300
20. Ziegler T, Rauk A. 1977. On the Calculation of Bonding Energies by the Hartree Fock Slater Method. *Theor. Chem. Acc.* 46:1–10
21. Ziegler T, Rauk A. 1979. A Theoretical Study of the Ethylene-Metal Bond in Complexes between Cu^+, Ag^+, Pt^0, or Pt^{2+} and Ethylene, Based on Hartree-Fock-Slater Transition-State Method. *Inorg. Chem.* 18:1558–1565
22. Bickelhaupt FM, Baerends EJ. 2007. Kohn-Sham Density Functional Theory: Predicting and Understanding Chemistry. In *Reviews in Computational Chemistry*, ed. KB Lipkowitz, DB Boyd, pp. 1–86, vol. 15. New York: John Wiley & Sons, Inc.
23. Mitoraj MP, Michalak A, Ziegler T. 2009. A Combined Charge and Energy Decomposition Scheme for Bond Analysis. *J. Chem. Theory Comput.* 5:962–975
24. Su P, Li H. 2009. Energy decomposition analysis of covalent bonds and intermolecular interactions. *J. Chem. Phys.* 131:014102
25. Su P, Jiang Z, Chen Z, Wu W. 2014. Energy Decomposition Scheme Based on the Generalized Kohn-Sham Scheme. *J. Phys. Chem. A* 118:2531–2542
26. Su P, Tang Z, Wu W. 2020. Generalized kohn-sham energy decomposition analysis and its applications. *WIREs: Comput. Mol. Sci.* :e1460
27. Mo Y, Gao J, Peyerimhoff SD. 2000. Energy decomposition analysis of intermolecular interactions using a block-localized wave function approach. *J. Chem. Phys.* 112:5530–5538
28. Mo Y, Song L, Lin Y. 2007. Block-Localized Wavefunction (BLW) Method at the Density Functional Theory (DFT) Level. *J. Phys. Chem. A* 111:8291–8301
29. Stoll H, Wagenblast G, Preuß H. 1980. On the Use of Local Basis Sets for Localized Molecular Orbitals. *Theor. Chem. Acc.* 57:169–178
30. Gianinetti E, Raimondi M, Tornaghi E. 1996. Modification of the Roothaan Equations to Exclude BSSE from Molecular Interaction Calculations. *Int. J. Quantum Chem.* 60:157–166
31. Khaliullin RZ, Head-Gordon M, Bell AT. 2006. An efficient self-consistent field method for large systems of weakly interacting components. *J. Chem. Phys.* 124:204105
32. Khaliullin RZ, Cobar EA, Lochan RC, Bell AT, Head-Gordon M. 2007. Unravelling the Origin of Intermolecular Interactions Using Absolutely Localized Molecular Orbitals. *J. Phys. Chem.*

A 111:8753–8765
33. Khaliullin RZ, Bell AT, Head-Gordon M. 2008. Analysis of charge transfer effects in molecular complexes based on absolutely localized molecular orbitals. *J. Chem. Phys.* 128:184112
34. Horn PR, Sundstrom EJ, Baker TA, Head-Gordon M. 2013. Unrestricted absolutely localized molecular orbitals for energy decomposition analysis: theory and applications to intermolecular interactions involving radicals. *J. Chem. Phys.* 138:134119
35. Ge Q, Mao Y, Head-Gordon M. 2018. Energy decomposition analysis for exciplexes using absolutely localized molecular orbitals. *J. Chem. Phys.* 148:064105
36. Ge Q, Head-Gordon M. 2018. Energy decomposition analysis for excimers using absolutely localized molecular orbitals within time-dependent density functional theory and configuration interaction with single excitations. *J. Chem. Theory Comput.* 14:5156–5168
37. Thirman J, Head-Gordon M. 2015. An energy decomposition analysis for second-order moller-plesset perturbation theory based on absolutely localized molecular orbitals. *J. Chem. Phys.* 143:084124
38. Thirman J, Head-Gordon M. 2017. Efficient implementation of energy decomposition analysis for second-order møller–plesset perturbation theory and application to anion–π interactions. *J. Phys. Chem. A* 121:717–728
39. Loipersberger M, Lee J, Mao Y, Das AK, Ikeda K, et al. 2019. Energy decomposition analysis for interactions of radicals: Theory and implementation at the mp2 level with application to hydration of halogenated benzene cations and complexes between $co_2^{-\bullet}$ and pyridine and imidazole. *J. Phys. Chem. A* 123:9621–9633
40. Azar RJ, Horn PR, Sundstrom EJ, Head-Gordon M. 2013. Useful lower limits to polarization contributions to intermolecular interactions using a minimal basis of localized orthogonal orbitals: theory and analysis of the water dimer. *J. Chem. Phys.* 138:084102
41. Horn PR, Head-Gordon M. 2015. Polarization contributions to intermolecular interactions revisited with fragment electric-field response functions. *J. Chem. Phys.* 143:114111
42. Lao KU, Herbert JM. 2016. Energy decomposition analysis with a stable charge-transfer term for interpreting intermolecular interactions. *J. Chem. Theory Comput.* 12:2569–2582
43. Jeziorski B, Moszynski R, Szalewicz K. 1994. Perturbation Theory Approach to Intermolecular Potential Energy Surfaces of van der Waals Complexes. *Chem. Rev.* 94:1887–1930
44. Misquitta AJ, Podeszwa R, Jeziorski B, Szalewicz K. 2005. Intermolecular potentials based on symmetry-adapted perturbation theory with dispersion energies from time-dependent density-functional calculations. *J. Chem. Phys.* 123:214103
45. Stone AJ, Misquitta AJ. 2009. Charge-transfer in Symmetry-Adapted Perturbation Theory. *Chem. Phys. Lett.* 473:201–205
46. Misquitta AJ. 2013. Charge Transfer from Regularized Symmetry-Adapted Perturbation Theory. *J. Chem. Theory Comput.* 9:5313–5326
47. Mao Y, Ge Q, Horn PR, Head-Gordon M. 2018. On the computational characterization of charge-transfer effects in noncovalently bound molecular complexes. *J. Chem. Theory Comput.* 14:2401–2417
48. Lao K, Schaffer R, Jansen G, Herbert J. 2015. Accurate description of intermolecular interactions involving ions using symmetry-adapted perturbation theory. *J. Chem. Theor. Comput.* 11:2473–2486
49. Glendening ED, Streitwieser A. 1994. Natural energy decomposition analysis: An energy partitioning procedure for molecular Interactions with application to weak hydrogen bonding, strong ionic, and moderate donor-acceptor interactions. *J. Chem. Phys.* 100:2900–2909
50. Glendening ED. 2005. Natural Energy Decomposition Analysis: Extension to Density Functional Methods and Analysis of Cooperative Effects in Water Clusters. *J. Phys. Chem. A* 109:11936–11940
51. Reed AE, Curtiss LA, Weinhold F. 1988. Intermolecular Interactions from a Natural Bond Orbital, Donor-Acceptor Viewpoint. *Chem. Rev.* 88:899–926

52. Stone AJ. 2017. Natural bond orbitals and the nature of the hydrogen bond. *J. Phys. Chem. A* 121:1531–1534
53. Khaliullin RZ, Bell AT, Head-Gordon M. 2009. Electron donation in the water–water hydrogen bond. *Chem.-Eur. J.* 15:851–855
54. Horn PR, Mao Y, Head-Gordon M. 2016. Defining the contributions of electrostatics, pauli repulsion and dispersion in density functional theory calculations of intermolecular interaction energies. *J. Chem. Phys.* 144:114107
55. Thirman J, Head-Gordon M. 2014. Electrostatic domination of the effect of electron correlation in intermolecular interactions. *J. Phys. Chem. Lett.* 5:1380–1385
56. Pernal K, Podeszwa R, Patkowski K, Szalewicz K. 2009. Dispersionless density functional theory. *Phys. Rev. Lett.* 103:263201
57. Zhang Y, Yang W. 1998. Comment on "generalized gradient approximation made simple". *Phys. Rev. Lett.* 80:890–890
58. Mardirossian N, Head-Gordon M. 2014. xB97X-V: A 10-parameter, range-separated hybrid, generalized gradient approximation density functional with nonlocal correlation, designed by a survival-of-the-fittest strategy. *Phys. Chem. Chem. Phys.* 16:9904–9924
59. Nagata T, Takahashi O, Saito K, Iwata S. 2001. Basis set superposition error free self-consistent field method for molecular interaction in multi-component systems: Projection operator formalism. *J. Chem. Phys.* 115:3553–3560
60. Weigend F, Ahlrichs R. 2005. Balanced basis sets of split valence, triple zeta valence and quadruple zeta valence quality for h to rn: Design and assessment of accuracy. *Phys. Chem. Chem. Phys.* 7:3297–3305
61. Prasad Veccham S, Head-Gordon M. 2020. (work in progress)
62. Mo Y. 2003. Geometrical optimization for strictly localized structures. *J. Chem. Phys.* 119:1300–1306
63. Loipersberger M, Mao Y, Head-Gordon M. 2020. Variational forward-backward charge transfer analysis based on absolutely localized molecular orbitals: Energetics and molecular properties. *J. Chem. Theory Comput.* 16:1073–1089
64. Ramos-Cordoba E, Lambrecht DS, Head-Gordon M. 2011. Charge-transfer and the hydrogen bond: Spectroscopic and structural implications from electronic structure calculations. *Farad. Discuss.* 150:345–362
65. Mao Y, Head-Gordon M. 2019. Probing blue-shifting hydrogen bonds with adiabatic energy decomposition analysis. *J. Phys. Chem. Lett.* 10:3899–3905
66. Hobza P, Havlas Z. 2002. Improper, blue-shifting hydrogen bond. *Theo. Chem. Acc.* 108:325–334
67. Hermansson K. 2002. Blue-shifting hydrogen bonds. *J. Phys. Chem. A* 106:4695–4702
68. Allen AD, Senoff CV. 1965. Nitrogenopentammineruthenium(ii) complexes. *Chem. Commun.* :621–622
69. Dewar J. 1951. A review of the pi-complex theory. *Bull. Soc. Chim. Fr.* 18:C71–C79
70. Chatt J, Duncanson LA. 1953. 586. olefin co-ordination compounds. part iii. infra-red spectra and structure: attempted preparation of acetylene complexes. *J. Chem. Soc.* :2939–2947
71. Herrmann WA. 1990. 100 years of metal carbonyls: a serendipitous chemical discovery of major scientific and industrial impact. *J. Organomet. Chem.* 383:21–44
72. Lupinetti AJ, Frenking G, Strauss SH. 1998. Nonclassical metal carbonyls: appropriate definitions with a theoretical justification. *Angew. Chem. Int. Ed.* 37:2113–2116
73. Rossomme EC, Lininger CN, Bell AT, Head-Gordon T, Head-Gordon M. 2020. Electronic structure calculations permit identification of the driving forces behind frequency shifts in transition metal monocarbonyls. *Phys. Chem. Chem. Phys.* 22:781–798
74. Drance MJ, Sears JD, Mrse AM, Moore CE, Rheingold AL, et al. 2019. Terminal coordination of diatomic boron monofluoride to iron. *Science* 363:1203–1205
75. Peverati R, Platt SP, Attah IK, Aziz SG, El-Shall MS, Head-Gordon M. 2017. Nucleophilic

aromatic addition in ionizing environments: Observation and analysis of new c–n valence bonds in complexes between naphthalene radical cation and pyridine. *J. Am. Chem. Soc.* 139:11923–11932
76. Lifson S, Warshel A. 1968. Consistent force field for calculations of conformations, vibrational spectra, and enthalpies of cycloalkane and n-alkane molecules. *J. Chem. Phys.* 49:5116–5129
77. Albaugh A, Boateng HA, Bradshaw RT, Demerdash ON, Dziedzic J, et al. 2016. Advanced potential energy surfaces for molecular simulation. *J. Phys. Chem. B* 120:9811–9832
78. Zgarbová M, Otyepka M, Šponer J, Hobza P, Jurečka P. 2010. Large-scale compensation of errors in pairwise-additive empirical force fields: comparison of amber intermolecular terms with rigorous dft-sapt calculations. *Phys. Chem. Chem. Phys.* 12:10476–10493
79. Halgren TA. 1992. Representation of van der waals (vdw) interactions in molecular mechanics force-fields - potential form, combination rules, and vdw parameters. *J. Am. Chem. Soc.* 114:7827–7843
80. Ren PY, Ponder JW. 2003. Polarizable atomic multipole water model for molecular mechanics simulation. *J. Phys. Chem. B* 107:5933–5947
81. Ponder JW, Wu C, Ren P, Pande VS, Chodera JD, et al. 2010. Current status of the amoeba polarizable force field. *J. Phys. Chem. B* 114:2549–2564
82. Wang LP, Head-Gordon T, Ponder JW, Ren P, Chodera JD, et al. 2013. Systematic improvement of a classical molecular model of water. *J. Phys. Chem. B* 117:9956–9972
83. Laury ML, Wang LP, Pande VS, Head-Gordon T, Ponder JW. 2015. Revised parameters for the amoeba polarizable atomic multipole water model. *J. Phys. Chem. B* 119:9423–9437
84. Warshel A, Kuwajima S. 1990. Incorporating electric polarizabilities in water-water interaction potentials. *J. Phys. Chem.* 94:460–466
85. Rick S, Stuart S, Berne B. 1994. Dynamical fluctuating charge force-fields: Application to liquid water. *J. Chem. Phys.* 101:6141–6156
86. Gao JL. 1997. Toward a molecular orbital derived empirical potential for liquid simulations. *J. Phys. Chem. B* 101:657–663
87. Lamoureux G, MacKerell AD, Roux B. 2003. A simple polarizable model of water based on classical drude oscillators. *J. Chem. Phy.* 119:5185–5197
88. Yu HB, Hansson T, van Gunsteren WF. 2003. Development of a simple, self-consistent polarizable model for liquid water. *J. Chem. Phys.* 118:221–234
89. Paesani F, Iuchi S, Voth GA. 2007. Quantum effects in liquid water from an ab initio-based polarizable force field. *J. Chem. Phys.* 127:074506
90. Huang J, Lopes PEM, Roux B, MacKerell AD. 2014. Recent advances in polarizable force fields for macromolecules: Microsecond simulations of proteins using the classical drude oscillator model. *J. Phys. Chem. Lett.* 5:3144–3150
91. Das AK, Demerdash ON, Head-Gordon T. 2018. Improvements to the amoeba force field by introducing anisotropic atomic polarizability of the water molecule. *J. Chem. Theory Comput.* 14:6722–6733
92. Lucas TR, Bauer BA, Patel S. 2012. Charge equilibration force fields for molecular dynamics simulations of lipids, bilayers, and integral membrane protein systems. *Biochimica et Biophysica Acta (BBA) - Biomembranes* 1818:318 – 329. Membrane protein structure and function
93. Lemkul JA, Huang J, Roux B, MacKerell Jr AD. 2016. An empirical polarizable force field based on the classical drude oscillator model: development history and recent applications. *Chem. Rev.* 116:4983–5013
94. Dykstra CE. 1993. Electrostatic interaction potentials in molecular force fields. *Chem. Rev.* 93:2339–2353
95. Demerdash O, Yap EH, Head-Gordon T. 2014. Advanced potential energy surfaces for condensed phase simulation. *Annu. Rev. Phys. Chem.* 65:149–74
96. Lopes PEM, Huang J, Shim J, Luo Y, Li H, et al. 2013. Polarizable force field for peptides and proteins based on the classical drude oscillator. *J. Chem. Theory Comput.* 9:5430–5449

97. Wang LP, Martinez TJ, Pande VS. 2014. Building force fields: An automatic, systematic, and reproducible approach. *J. Phys. Chem. Lett.* 5:1885–1891
98. Wang LP, McKiernan KA, Gomes J, Beauchamp KA, Head-Gordon T, et al. 2017. Building a more predictive protein force field: A systematic and reproducible route to amber-fb15. *J. Phys. Chem. B* 121:4023–4039
99. Demerdash O, Mao Y, Liu T, Head-Gordon M, Head-Gordon T. 2017. Assessing many-body contributions to intermolecular interactions of the amoeba force field using energy decomposition analysis of electronic structure calculations. *J. Chem. Phys.* 147:161721
100. Stone AJ. 1993. Computation of charge-transfer energies by perturbation theory. *Chem. Phys. Lett.* 211:101–109
101. Demerdash ON, Head-Gordon T. 2016. Convergence of the many-body expansion for energy and forces for classical polarizable models in the condensed phase. *J. Chem. Theory Comput.* in press
102. Das AK, Urban L, Leven I, Loipersberger M, Aldossary A, et al. 2019. Development of an advanced force field for water using variational energy decomposition analysis. *J. Chem. Theory Comput.* 15:5001–5013
103. Mao Y, Demerdash O, Head-Gordon M, Head-Gordon T. 2016. Assessing ion-water interactions in the amoeba force field using energy decomposition analysis of electronic structure calculations. *J. Chem. Theory Comput.* 12:5422–5437
104. Mao Y, Shao Y, Dziedzic J, Skylaris CK, Head-Gordon T, Head-Gordon M. 2017. Performance of the amoeba water model in the vicinity of qm solutes: A diagnosis using energy decomposition analysis. *J. Chem. Theory Comput.* 13:1963–1979
105. Demerdash O, Wang LP, Head-Gordon T. 2018. Advanced models for water simulations. *WIRES: Comput. Mol. Sci.* 8:e1355
106. Piquemal JP, Gresh N, Giessner-Prettre C. 2003. Improved formulas for the calculation of the electrostatic contribution to the intermolecular interaction energy from multipolar expansion of the electronic distribution. *J. Phys. Chem. A* 107:10353–10359
107. Wang Q, Rackers JA, He C, Qi R, Narth C, et al. 2015. General model for treating short-range electrostatic penetration in a molecular mechanics force field. *J. Chem. Theory Comput.* 11:2609–2618
108. Rackers JA, Wang Q, Liu C, Piquemal JP, Ren P, Ponder JW. 2017. An optimized charge penetration model for use with the amoeba force field. *Phys. Chem. Chem. Phys.* 19:276–291
109. Jakobsen S, Jensen F. 2016. Searching the force field electrostatic multipole parameter space. *J. Chem. Theory Comput.* 12:1824–1832
110. Piquemal JP, Chelli R, Procacci P, Gresh N. 2007. Key role of the polarization anisotropy of water in modeling classical polarizable force fields. *J. Phys. Chem. A* 111:8170–8176
111. Brookes DH, Head-Gordon T. 2015. Family of oxygen–oxygen radial distribution functions for water. *J. Phys. Chem. Lett.* 6:2938–2943
112. Babin V, Leforestier C, Paesani F. 2013. Development of a "first principles" water potential with flexible monomers: Dimer potential energy surface, vrt spectrum, and second virial coefficient. *J. Chem. Theory Comput.* 9:5395–5403
113. Babin V, Medders GR, Paesani F. 2014. Development of a "first principles" water potential with flexible monomers. ii: Trimer potential energy surface, third virial coefficient, and small clusters. *J. Chem. Theory Comput.* 10:1599–1607
114. Levine DS, Horn PR, Mao Y, Head-Gordon M. 2016. Variational energy decomposition analysis of chemical bonding. 1. spin-pure analysis of single bonds. *J. Chem. Theory Comput.* 12:4812–4820
115. Levine DS, Head-Gordon M. 2017. Energy decomposition analysis of single bonds within kohn–sham density functional theory. *Proc. Natl. Acad. Sci. U.S.A* 114:12649–12656
116. Mao Y, Loipersberger M, Kron KJ, Sharada SM, Head-Gordon M. 2020. (work in progress)